

Counter-propagating charge transport in the quantum Hall effect regime

Fabien Lafont^{1,2,*}, Amir Rosenblatt^{1,*}, Moty Heiblum¹, Vladimir Umansky¹

¹*Braun Center for Submicron Research, Dept. of Condensed Matter physics, Weizmann Institute of Science, Rehovot 76100, Israel*

²*Collège de France, 11 place Marcelin Berthelot, 75231 Paris Cedex 05, France and*

**These authors contributed equally to this work*

The quantum Hall effect, observed in a two-dimensional electron gas subjected to a perpendicular magnetic field, imposes a 1D-like chiral, downstream, transport of charge carriers along the sample edges. Although this picture remains valid for electrons and Laughlin's fractional quasiparticles, it no longer holds for quasiparticles in the so-called hole-conjugate states. These states are expected, when disorder and interactions are weak, to harbor upstream charge modes. However, so far, charge currents were observed to flow exclusively downstream in the quantum Hall regime. Studying the canonical spin-polarized and spin-unpolarized $\nu = 2/3$ hole-like states in GaAs-AlGaAs heterostructures, we observed a significant upstream charge current at short propagation distances in the spin unpolarized state.

Elementary charge excitations in the quantum Hall effect (QHE) flow downstream along the edge of a two-dimensional electron gas (2DEG), with the downstream chirality imposed by the magnetic field [1]. In the fractional regime [2] this statement remains valid only for particle-like (Laughlin's) states [3–5]; in contrast, hole-like states (filling factors ν such that $1/2 + n < \nu < 1 + n$ with $n = 0, 1, 2, \dots$), are expected to harbor counter-propagating (downstream and upstream) charge excitations [6]. In a non-interacting and scattering-free model, a downstream $\nu = 1$ charge mode was predicted to be accompanied by an upstream $\nu = 1/3$ mode, leading to a two-terminal conductance of $4e^2/3h$ where e and h are respectively the electron charge and the Planck constant. However, experimentally, only downstream charge modes [7, 8] with a two-terminal conductance of $2e^2/3h$ accompanied by upstream neutral modes [9–15] have been found. A recent experiment [16] measured conductance of an unequilibrated downstream channels at narrow regions ($4 \mu\text{m}$ wide) of the polarized $\nu = 2/3$ state; the results were consistent with the model from [6] but no direct measurement of the upstream current was made. Although the majority of the studies were concentrated on the spin-polarized $\nu = 2/3$ state, there has been recent interest in its spin-unpolarized counterpart [17–24] - as a potential host for para-fermions when coupled to superconducting contacts [25–27]. In the Composite Fermion (CF) picture, one can construct two kinds of states in the $\nu = 2/3$: An unpolarized state, emerging at lower magnetic fields, with two quantum levels that have the same orbital quantum number

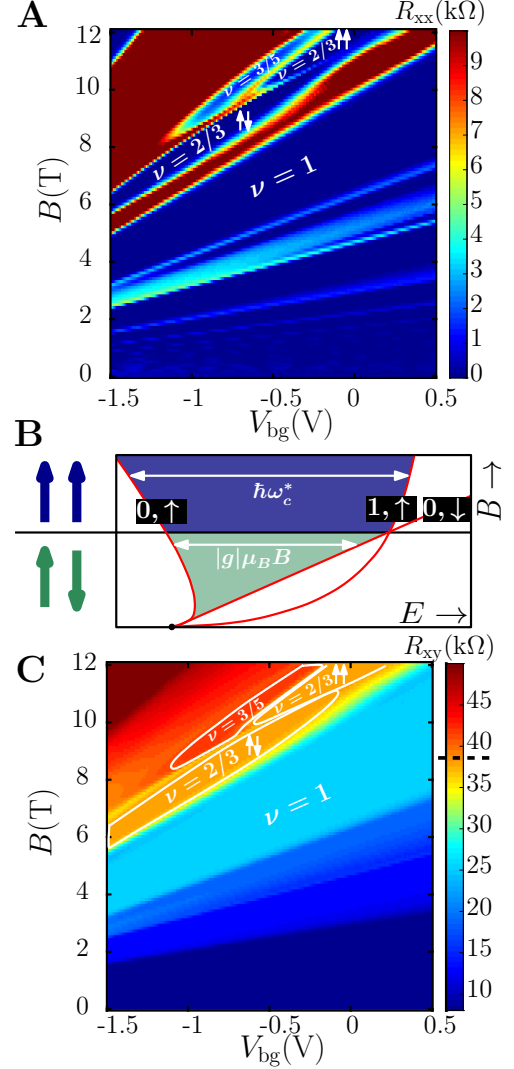


Figure 1. **Longitudinal and transverse magnetoresistances measured in a $40 \mu\text{m}$ wide Hall bar sample.** (A) Longitudinal four-terminal magneto-resistance versus backgate voltage measured using $I = 1 \text{ nA}$ at $T = 40 \text{ mK}$. A clear non-dissipated state, $R_{xx} \approx 0$, is visible for the $\nu = 2/3$ polarized and unpolarized states. (B) Sketch of the evolution of the relevant energy scales: At low field a gap exists between the $(0, \uparrow)$ and $(0, \downarrow)$ states corresponding to the spin unpolarized state), whereas at higher fields, thanks to the different B dependency of the Coulomb ($\propto l_B^{-1} \sim \sqrt{B}$, where l_B is the magnetic length) and Zeeman ($\propto B$) energies, the gap exists between the $(0, \uparrow)$ and the $(1, \uparrow)$ lambda levels corresponding to the polarized state. (C) Four-terminal transverse magneto-resistance as function of the backgate voltage. The $\nu = 2/3$ polarized and unpolarized quantum Hall plateaus exhibit a resistance $R_{xy} \approx (3e^2/2h)^{-1} \approx 38.7 \text{ k}\Omega$ (dashed line on the color bar).

but opposite spin configurations: $(0, \uparrow)$ and $(0, \downarrow)$ (Fig. 1B) [28], and a polarized state, emerging at high magnetic fields, with two quantum levels having the same spin but different orbitals $(0, \uparrow)$ and $(1, \uparrow)$ [29]. The majority of previous experiments in the unpolarized state focused on characterizing the spin domains structure in the bulk [23, 24, 30] or the nuclear spin polarization occurring at high currents [18, 19, 22, 30–36]. Still, the configuration of edge channels for this state remains elusive: on the one hand, no upstream channel is expected in the CF picture, on the other, because the effective K-Matrix in the CF basis is the same for both $\nu = 2/3$ states, an upstream mode should occur also in the unpolarized case [37]. Here, we studied the two flavors of the $\nu = 2/3$ state along short distance (a few μm) and found a substantial upstream charge current only in the spin-unpolarized state. Consequently, the two-terminal resistance deviates from the quantized one at $\nu = 2/3$. The GaAs-AlGaAs heterostructure used to study the two $\nu = 2/3$ states had to be carefully designed (with the 2DEG confined in a narrow, 12 nm wide, quantum-well), as we aimed to have the transition between the two states at a sufficiently high carrier density (and magnetic field), corresponding to having high mobility throughout the transition region in the phase space between the two states. A conductive n^+ GaAs layer was grown $\sim 1 \mu\text{m}$ below the 2DEG and served as a backgate, capable of tuning the density from 1 to $2.5 \times 10^{11} \text{ cm}^{-2}$, with a corresponding low temperature dark mobility of 1.5 to $3.5 \times 10^6 \text{ cm}^2 \text{ V}^{-1} \text{ s}^{-1}$. Lock-in measurements were performed at $\sim 80 \text{ Hz}$ with an input current $I = 1 \text{ nA}$ and an electron temperature of $\sim 35 \text{ mK}$ (see section 1 of [38] for additional fabrication information).

The evolution of the four-terminal longitudinal (R_{xx}), and transverse resistance (R_{xy}), measured in a $40 \mu\text{m}$ wide Hall-bar geometry, is plotted on Fig. 1A and C. As reported previously [17, 22, 30–32], a clear transition between the two-spin varieties of the $\nu = 2/3$ states is visible in R_{xx} (around $V_{\text{bg}} = -0.5 \text{ V}$ and $B = 10 \text{ T}$ in Fig. 1A). The finite R_{xx} region corresponds to the point where the system undergoes a first order quantum phase transition between the spin unpolarized and the spin polarized $\nu = 2/3$ state. The transverse resistance $R_{xy} \simeq (2/3 e^2/h)^{-1} \simeq 38.7 \text{ k}\Omega$, however, remains constant on both side of the transition. As predicted in [6] the presence of an upstream current leads to the deviation of the two-terminal resistance from the canonical value $R_{2t} \simeq 38.7 \text{ k}\Omega$. We therefore have conducted two-terminal resistance measurements of several samples, consisting of two $60 \mu\text{m}$ -wide ohmic contacts separated by a distance L ranging from 4 to $15 \mu\text{m}$. The large aspect ratio (of width to length) minimizes backscattering between the propagating edge modes on opposite sides of the mesa. As visible on Fig. 2A for $L = 4 \mu\text{m}$, in the (B, V_{bg}) phase space corresponding to the polarized state, we find a two-terminal resistance $R_{2t}^{\uparrow\uparrow}(L = 4) \simeq 38.6 \pm 0.1 \text{ k}\Omega$. However, for the unpolarized state, the resistance plateau is found to deviate from

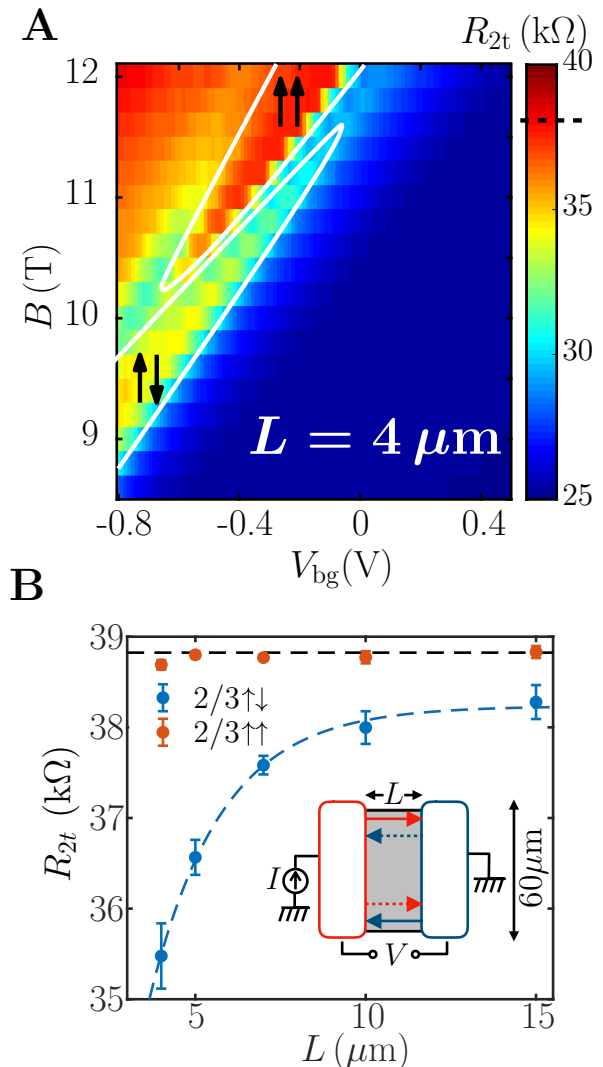


Figure 2. **Deviation from the quantized Hall resistance value owing to the upstream current.** (A) Two-terminal magneto-resistance versus backgate voltage for a $L = 4 \mu\text{m}$ long and $60 \mu\text{m}$ wide sample measured at $T \sim 35 \text{ mK}$ and $I = 1 \text{ nA}$. A clear difference appears between the spin-polarized state, which remains quantized, and the spin unpolarized state, which deviates substantially from the quantized value. (B) Evolution of the two-terminal resistance averaged over an area of (B, V_{bg}) corresponding to the polarized and unpolarized $\nu = 2/3$ states, as a function of the length L (see section 2 of [38]). Dashed black line is the quantized value $(2/3 e^2/h)^{-1}$ and dashed blue line is an exponential fit $R(x) = (R(0) - R(\infty)) e^{-x/l_0} + R(\infty)$, where $R(0) = 20 \pm 13 \text{ k}\Omega$, $R(\infty) = 38.2 \pm 0.3 \text{ k}\Omega$ and $l_0 = 2.1 \pm 0.8 \mu\text{m}$

the quantized value showing $R_{2t}^{\downarrow\downarrow}(L = 4) \simeq 35.5 \text{ k}\Omega$.

Measuring the evolution of $R_{2t}^{\uparrow\uparrow}$ and $R_{2t}^{\downarrow\downarrow}$ with length we find $R_{2t}^{\uparrow\uparrow}$ independent of contact separation (Fig. 2B, orange circles) whereas $R_{2t}^{\downarrow\downarrow}$ increases with L , approaching the quantized value for $L=15 \mu\text{m}$ (Fig. 2B, blue circles). Exponential fit of the two-terminal resistance is

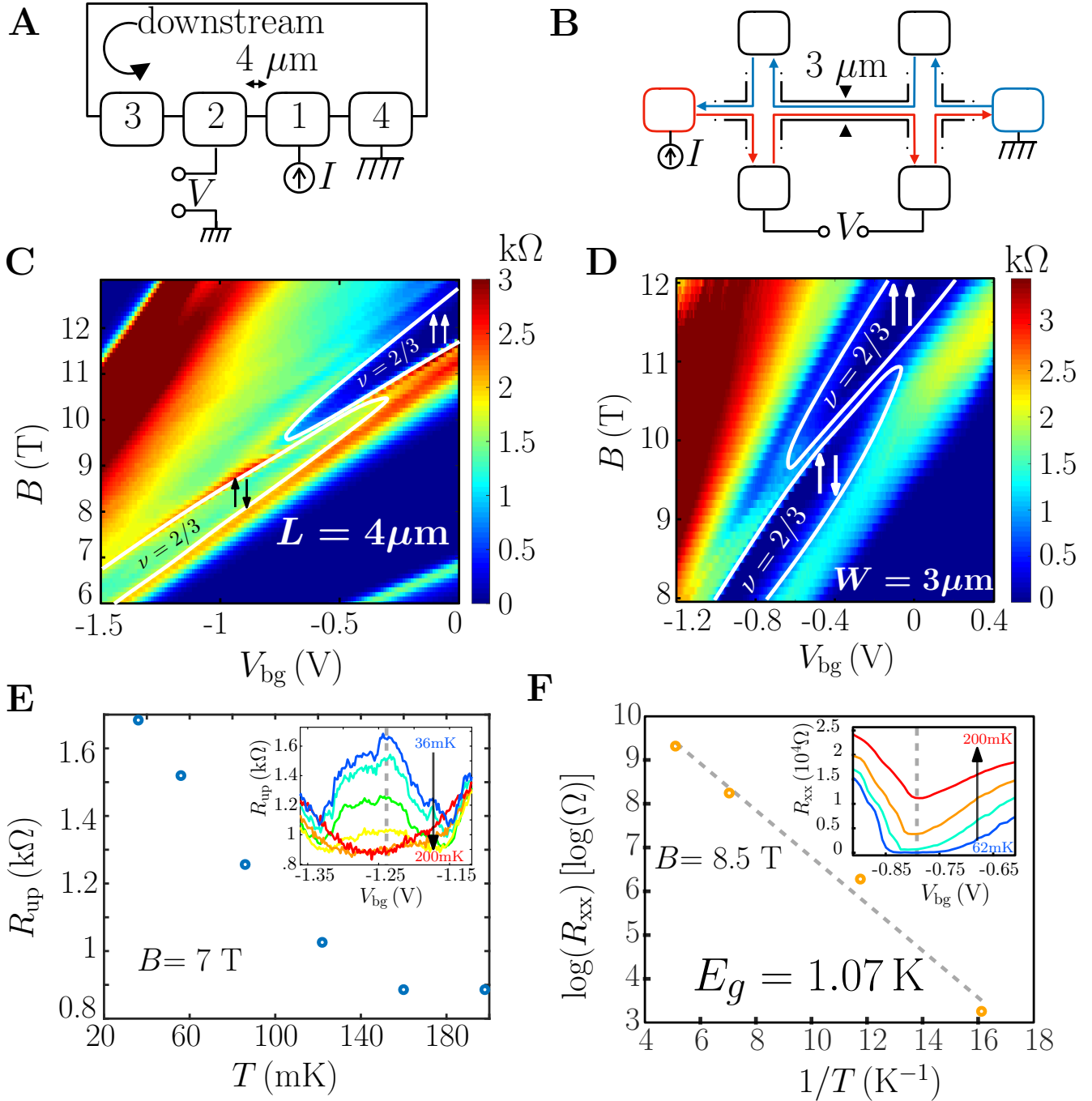


Figure 3. **Different sample geometries validating the presence of a counter propagating charge flow.** (A) Sketch of the 3-terminal measurement. Four contacts are aligned on a single edge of the sample $4 \mu\text{m}$ apart. Current $I = 1$ nA was sourced at contact 1 and voltage was measured between the contact 2 placed upstream and the ground; contact 4 was grounded and contact 3 was floating. (B) Sketch of the 4-terminal R_{xx} measurement on a narrow, $3 \mu\text{m}$ wide and $25 \mu\text{m}$ long Hall bar. The red lines represent the biased edge channels whereas the blue ones represent the grounded edge channels. (C) 3-terminal magnetoresistance versus the backgate voltage for the measurement scheme presented in (A), a clear finite resistance appears in the unpolarized region. (D) 4-terminal R_{xx} versus backgate voltage for the measurement scheme presented in (B). The R_{xx} values are low in both polarized and unpolarized regions, in contrast to (C). (E) Evolution of the resistance measured in the unpolarized regime at $B = 7$ T and $V_{bg} = -1.24$ V as function of temperature. Inset: Resistance in the unpolarized regime as function of the backgate voltage for different temperatures (36, 56, 86, 122, 160 and 198 mK). (F) Evolution of the log of the longitudinal resistance versus the inverse of the temperature in the Hall bar geometry. Inset: Evolution of the resistance versus the backgate voltage in the unpolarized regime for several temperatures (62, 85, 142 and 196 mK). The extracted activation gap is $E_g = 1.07$ K

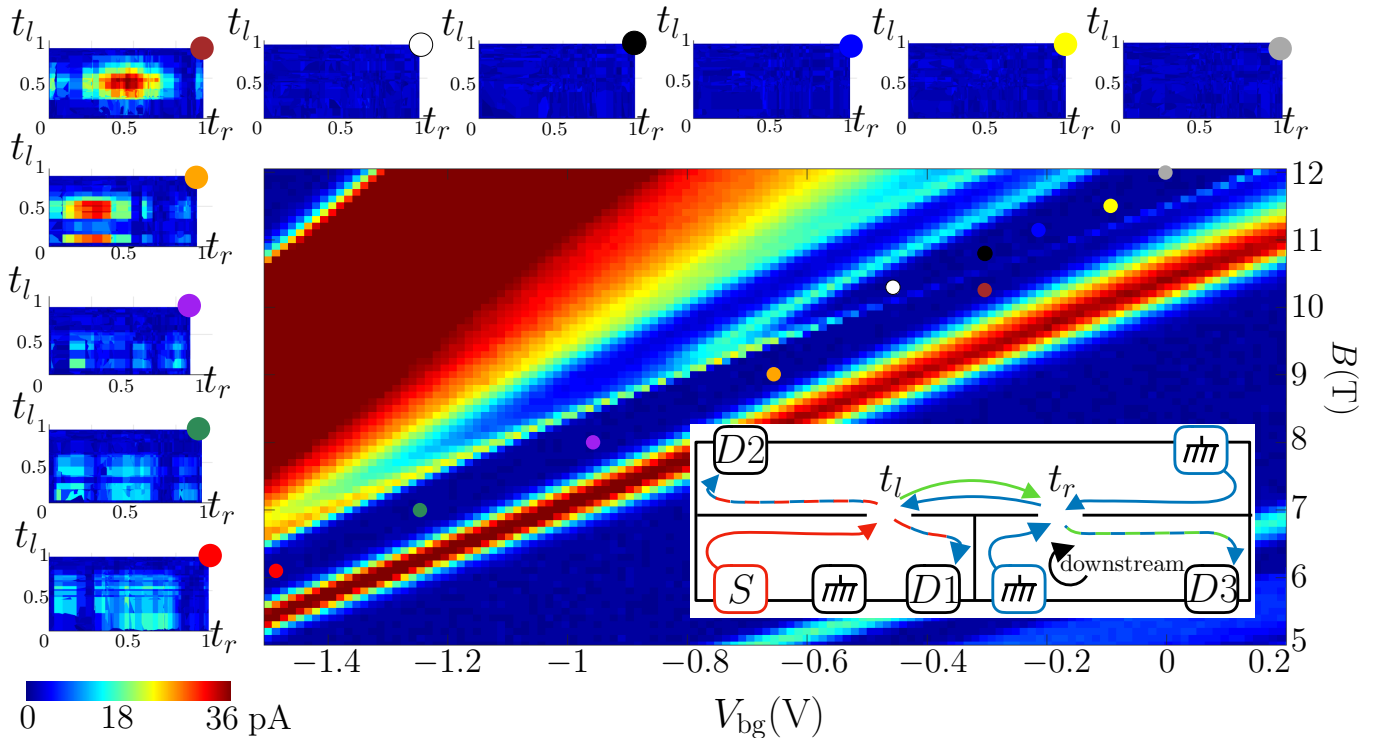


Figure 4. **Generation of upstream charge current by a quantum point contact.** Evolution of the current measured in $D3$ as function of t_l and t_r for different points in the (V_{bg}, B) phase space (points shown in the main panel). A significant current is measurable in the unpolarized region (red, green, purple, orange and brown points) whereas no signal was measurable in the polarized region (white, black, blue, yellow and gray points). Inset: Two successive quantum point contacts setup. Current is sourced at S (red), flowing downstream to the left QPC; there, it is split to downstream (red/blue) and upstream (green) charge currents. The unequilibrated upstream current reaches the second QPC and turns back to downstream (green/blue), where we measure its voltage at $D3$. The sketch is not to scale, the distance between the two QPC is 700 nm and the distance between the QPC and the nearest ohmic contact is $30 \text{ }\mu\text{m}$.

presented in Fig. 2B (dashed blue line), $R(x) = (R(0) - R(\infty) \exp(-x/l_0) + R(\infty))$, where $R(0) = 20 \pm 13 \text{ k}\Omega$ is the resistance at zero distance, $R(\infty) = 38.2 \pm 0.3 \text{ k}\Omega$ is the resistance at infinite distance, $l_0 = 2.1 \pm 0.8 \text{ }\mu\text{m}$ is the characteristic equilibration length (see section 2 of [38] for additional details on Fig. 2B). Moreover, it is worth noting that the resistance $R(0)$ is in agreement with the two-terminal resistance predicted for unequilibrated channels proposed in [6], $R_{2t} = (4/3 e^2/h)^{-1} \approx 19.4 \text{ k}\Omega$. These observations might have been possible at short distance due to the reduction of scattering events and the screening of the Coulomb interaction by the back gate placed $1 \text{ }\mu\text{m}$ away from the 2DEG.

Bearing in mind that a finite R_{xx} caused by dissipation processes at short contact separation can lead to similar observations, a few additional configurations were tested. One of them was a configuration that employs a complementary Hall bar structure, with a narrow Hall channel width of $3 \text{ }\mu\text{m}$ (Fig. 3B); this was necessary in order to ensure the lack of backscattering along distances under consideration. The measured R_{xx} (Fig. 3D) for the two $\nu = 2/3$ states using this geometry was negligibly small ensuring that edge states located on opposite

sides of the Hall bar (red and blue lines on Fig. 3B) do not exchange particles. This observation is in agreement with the relatively large gap ($\sim 1 \text{ K}$ for the unpolarized state) extracted from the temperature evolution of R_{xx}^{4p} presented on Fig. 3F, and in agreement with previous measurements [39, 40]. Furthermore, testing a Corbino geometry sample ensured a negligible bulk conductance of both $\nu = 2/3$ states (see section 3 of [38]). Finally, a three-terminal configuration, with contacts aligned on a single edge of the mesa (each separated by $4 \text{ }\mu\text{m}$), allowed to separate the upstream current from the downstream one (Fig. 3A), providing a direct measurement for the upstream conductance. Current I was sourced via contact 1 and drained via contact 4 to the ground. A finite voltage V_{up} was measured at contact 2 for the unpolarized state only as visible on Fig. 3C. The resistance, defined as $R_{up} = V_{up}/I$, continuously dropped with increasing temperature up to 200 mK (Fig. 3E). This dependence has an opposite trend to that of usual dissipative processes such as variable range hopping or activation mechanisms, ruling them out as alternative explanations. A complementary measurement of the downstream resistance, $R_d = V_d/I$, was done by sourcing cur-

rent via contact 2 and measuring the voltage at contact 1. The upstream and downstream conductances, calculated using the Landauer - Buttiker formalism [41, 42] (see section 4 of [38]), leads to $G_d \approx 0.687 e^2/h$ and $G_{up} \approx 0.026 e^2/h$ or equivalent to a two-terminal resistance $(G_{up} + G_d)^{-1} \approx 1.40 h/e^2 \approx 36.2 k\Omega$, in agreement with the two-terminal configuration at $4 \mu\text{m}$ presented above (in Fig. 2). The mobility of the 2DEG in proximity to an alloyed ohmic contact is degraded and its density is increased, which limited us on the minimal distance between ohmic contacts to $4 \mu\text{m}$. In order to probe the edge modes at shorter distances we employed a configuration consisting of two, gate defined quantum point contacts (QPCs) separated by 700 nm shown in Fig. 4, inset, with all ohmic contacts placed far away (above $30 \mu\text{m}$). A current $I = 1 \text{ nA}$ was sourced via contact S ; currents were monitored at the drains while scanning the transmissions of the left and right QPCs t_l and t_r . This was done at different points in the (V_{bg}, B) phase space for both spin polarization of the $\nu = 2/3$ states, indicated by the colored circles in Fig. 4. In the polarized state, all of the current flowed to drains $D1$ and $D2$ independent of t_r , consistent with downstream channels and zero current was measured at $D3$ (white, black, blue, yellow and gray points in Fig. 4). However, in the unpolarized state (red, green, purple, orange and brown points in Fig. 4), substantial signal was found in $D3$, simultaneously decreasing the current measured in $D1$ and $D2$ result in overall current conservation (see section 5 of [38]). This ‘upstream effect’ can be explained by the appearance of an upstream current between the two QPCs (green arrow in Fig. 4 inset), which emerges from the left QPC, flows a short distance to the right QPC, and scatters back to

the downstream channel, finally arriving at $D3$. Interestingly, a maximum current at $D3$ was measured when $t_l = t_r = 0.5$ (a toy model for this effect is presented in Section 6 of [38]).

The present set of experiments revealed counter-propagation of charged particles in the fractional quantum Hall effect regime. This present experiment may induce future theoretical works of the less understood unpolarized $\nu = 2/3$ state.

Acknowledgements: We thank Ady Stern and Yigal Meir for fruitful discussions. We would like to thank Diana Mahalu for her precious help in the ebeam lithography process. **Funding:** We acknowledge the European Research Council under the European Community’s Seventh Framework Program, grant agreement number 339070, the partial support of the Minerva Foundation, grant number 711752, and, together with V.U., the German Israeli Foundation (GIF), grant number I-1241-303.10/2014, and the Israeli Science Foundation (ISF). **Author contributions:** F.L. and A.R. contributed equally to this work in sample design, device fabrication, measurement set-up, data acquisition, data analysis and interpretation, and writing of the paper. M.H. guided the experimental work and contributed in data interpretation and writing of the paper. V.U. contributed in molecular beam epitaxy growth. **Competing interests:** The authors declare that they have no competing financial interests. **Data and materials availability:** All data needed to evaluate the conclusions in the paper are present in the paper or the supplementary materials. Additional data will be provided upon reasonable request to the corresponding author.

-
- [1] K. V. Klitzing, G. Dorda, and M. Pepper, Physical Review Letters **45**, 494 (1980).
- [2] D. C. Tsui, H. L. Stormer, and A. C. Gossard, Physical Review Letters **48**, 1559 (1982).
- [3] R. B. Laughlin, Physical Review Letters **50**, 1395 (1983).
- [4] C. W. J. Beenakker, Physical Review Letters **64**, 216 (1990).
- [5] X. Wen, Modern Physics Letters B **05**, 39 (1991).
- [6] A. H. MacDonald, Physical Review Letters **64**, 220 (1990).
- [7] R. C. Ashoori, H. L. Stormer, L. N. Pfeiffer, K. W. Baldwin, and K. West, Physical Review B **45**, 3894 (1992).
- [8] R. Sabo, I. Gurman, A. Rosenblatt, F. Lafont, D. Banitt, J. Park, M. Heiblum, Y. Gefen, V. Umansky, and D. Mahalu, Nature Physics (2017), 10.1038/nphys4010.
- [9] C. L. Kane, M. P. A. Fisher, and J. Polchinski, Physical Review Letters **72**, 4129 (1994).
- [10] Y. Meir, Physical Review Letters **72**, 2624 (1994).
- [11] J. Wang, Y. Meir, and Y. Gefen, 10.1103/PhysRevLett.111.246803.
- [12] A. Bid, N. Ofek, H. Inoue, M. Heiblum, C. L. Kane, V. Umansky, and D. Mahalu, Nature **466**, 585 (2010).
- [13] I. Gurman, R. Sabo, M. Heiblum, V. Umansky, and D. Mahalu, Nature Communications **3**, 1289 (2012).
- [14] H. Inoue, A. Grivnin, Y. Ronen, M. Heiblum, V. Umansky, and D. Mahalu, Nature Communications **5** (2014), 10.1038/ncomms5067.
- [15] A. Rosenblatt, F. Lafont, I. Levkivskiy, R. Sabo, I. Gurman, D. Banitt, M. Heiblum, and V. Umansky, Nature communications **8**, 2251 (2017).
- [16] A. Grivnin, H. Inoue, Y. Ronen, Y. Baum, M. Heiblum, V. Umansky, and D. Mahalu, Phys. Rev. Lett. **113**, 266803 (2014).
- [17] J. P. Eisenstein, H. L. Stormer, L. N. Pfeiffer, and K. W. West, Physical Review B **41**, 7910 (1990).
- [18] S. Kronmüller, W. Dietsche, J. Weis, K. von Klitzing, W. Wegscheider, and M. Bichler, Physical Review Letters **81**, 2526 (1998).
- [19] S. Kronmüller, W. Dietsche, K. v. Klitzing, G. Denninger, W. Wegscheider, and M. Bichler, Physical Review Letters **82**, 4070 (1999).
- [20] T. Chakraborty, Advances in Physics **49**, 959 (2000).
- [21] J. H. Smet, R. A. Deutschmann, W. Wegscheider, G. Abstreiter, and K. von Klitzing, Physical Review Letters **86**, 2412 (2001).
- [22] S. Kraus, O. Stern, J. G. S. Lok, W. Dietsche, K. Von

- Klitzing, M. Bichler, D. Schuh, and W. Wegscheider, **21**, 10.1103/PhysRevLett.89.266801.
- [23] J. Hayakawa, K. Muraki, and G. Yusa, *Nature Nanotechnology* **8**, 31 (2012).
- [24] J. N. Moore, J. Hayakawa, T. Mano, T. Noda, and G. Yusa, *Phys. Rev. Lett.* **118**, 076802 (2017).
- [25] R. S. K. Mong, D. J. Clarke, J. Alicea, N. H. Lindner, P. Fendley, C. Nayak, Y. Oreg, A. Stern, E. Berg, K. Shtengel, and M. P. A. Fisher, *Physical Review X* **4** (2014), 10.1103/PhysRevX.4.011036, arXiv:1307.4403.
- [26] D. J. Clarke, J. Alicea, and K. Shtengel, *Nature Physics* **10**, 877 (2014), arXiv:1312.6123.
- [27] T. Wu, Z. Wan, A. Kazakov, Y. Wang, G. Simion, J. Liang, K. W. West, K. Baldwin, L. N. Pfeiffer, Y. Lyanda-Geller, and L. P. Rokhinson, *Phys. Rev. B* **97**, 245304 (2018).
- [28] J. K. Jain, *Physical Review Letters* **63**, 199 (1989).
- [29] I. V. Kukushkin, K. V. Klitzing, and K. Eberl, **82** (1999).
- [30] B. Verdene, J. Martin, G. Gamez, J. Smet, K. von Klitzing, D. Mahalu, D. Schuh, G. Abstreiter, and A. Yacoby, *Nature Physics* **3**, 392 (2007).
- [31] J. H. Smet, R. A. Deutschmann, W. Wegscheider, G. Abstreiter, and K. Von Klitzing, *Physical Review Letters* **86**, 2412 (2001).
- [32] J. Huels, J. Weis, J. Smet, K. Klitzing, and Z. Wasilewski, *Physical Review B* **69**, 085319 (2004).
- [33] S. Hennel, B. A. Braem, S. Baer, L. Tiemann, P. Sohi, D. Wehrli, A. Hofmann, C. Reichl, W. Wegscheider, C. Rössler, T. Ihn, K. Ensslin, M. S. Rudner, and B. Rosenow, *Phys. Rev. Lett.* **116**, 136804 (2016).
- [34] H. Cho, J. B. Young, W. Kang, K. L. Campman, A. C. Gossard, M. Bichler, and W. Wegscheider, *Phys. Rev. Lett.* **81**, 2522 (1998).
- [35] Y. Q. Li, V. Umansky, K. von Klitzing, and J. H. Smet, *Phys. Rev. B* **86**, 115421 (2012).
- [36] J. H. Smet, R. A. Deutschmann, F. Ertl, W. Wegscheider, G. Abstreiter, and K. von Klitzing, *Nature* **415**, 281 (2002).
- [37] Y.-H. Wu, G. J. Sreejith, and J. K. Jain, *Phys. Rev. B* **86**, 115127 (2012).
- [38] *Supplementary Materials*.
- [39] L. W. Engel, S. W. Hwang, T. Sajoto, D. C. Tsui, and M. Shayegan, *Physical Review B* **45**, 3418 (1992).
- [40] G. S. Boebinger, A. M. Chang, H. L. Stormer, and D. C. Tsui, *Physical Review Letters* **55**, 1606 (1985).
- [41] M. Büttiker, *Physical Review Letters* **57**, 1761 (1986).
- [42] S. Datta, *Cambridge University Press*, Vol. 3 (1995) p. 377.

Counter-propagating charge transport in the quantum Hall effect regime

Supplementary text

Fabien Lafont^{1,2,*}, Amir Rosenblatt^{1,*}, Moty Heiblum¹, Vladimir Umansky¹

¹*Braun Center for Submicron Research, Dept. of Condensed Matter physics,
Weizmann Institute of Science, Rehovot 76100, Israel*

²*Collège de France, 11 place Marcelin Berthelot, 75231 Paris Cedex 05, France and*

**These authors contributed equally to this work*

1. Sample fabrication

A narrow quantum well (12nm) is buried 83 nm below the surface of a GaAs-AlGaAs heterostructure. A conductive n^+ layer of GaAs was grown $\sim 1\mu\text{m}$ below the 2DEG and served as a back-gate. A window etched $\sim 0.9\mu\text{m}$ deep, followed by evaporation of 110 nm Au, 55 nm Ge and 40 nm Ni alloyed to the heterostructure, give us a connection to the back-gate. The same evaporation, on top of the heterostructure, also produce the ohmic contacts. The QPCs were defined by split metallic gates consisting of 5 nm Ti and 15 nm Au evaporated on the GaAs-AlGaAs heterostructure. The opening of each QPC is 500 nm wide.

2. Two-terminal measurements

Two-terminal magneto-resistance measurements were made on $60\mu\text{m}$ wide mesa contacted by two ohmic contacts separated by a distance L ranging from 4 to $15\mu\text{m}$. Current $I = 1\text{nA}$ was sourced in one contact and drained to ground from the other contact while their voltage difference was monitored. Quantum Hall edge states are formed at the edges of the sample as sketched in Fig. S1A: solid arrows illustrate downstream (clockwise) chiral modes and dashed arrows illustrate the upstream charge transport on the edge. Two-terminal resistance $R_{2t} = V/I$ were measured as function of magnetic field and backgate voltage on five separate devices as shown in Fig. S1B-F. We extracted a mean value of R_{2t} from each plot shown in Sup 1F, averaged over the area in the (B, V_{bg}) phase-space corresponding to each state. R_{2t} of the unpolarized state approaches the quantized value at long L and goes down as L decrease, we fitted the data set using an exponential fit: $R(x) = (R(0) - R(\infty)) e^{-x/l_0} + R(\infty)$, where $R(0) = 20 \pm 13\text{ k}\Omega$ is the value at zero distance, $R(\infty) = 38.2 \pm 0.3\text{ k}\Omega$ is the value at infinite distance and $l_0 = 2.1 \pm 0.8\mu\text{m}$ is the typical equilibration length. Note that the zero distance resistance is in agreement with the model presented in [3] for noninteracting edge channels where $R_{2t} = (4/3 e^2/h)^{-1} = 19.4\text{ k}\Omega$

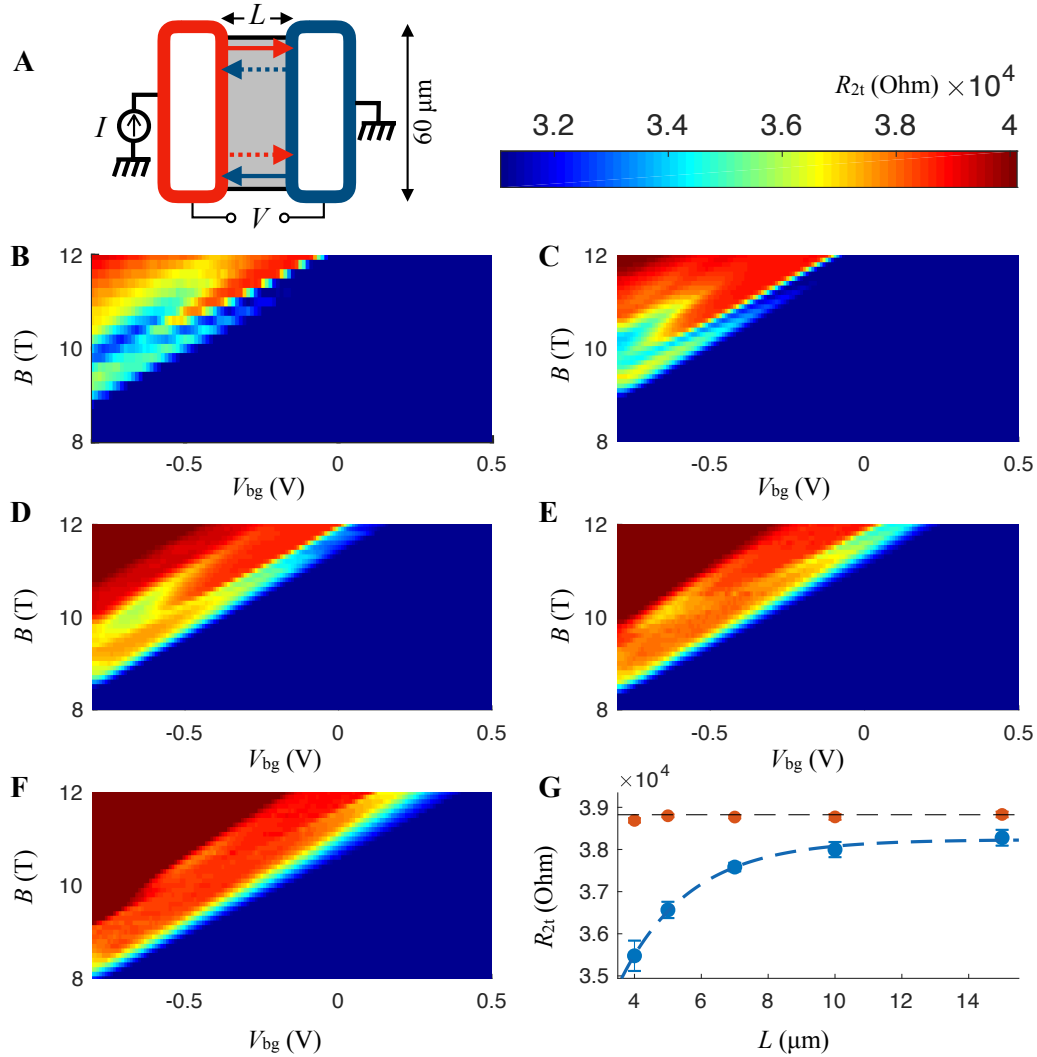


Figure 1: **Two-terminal magneto-resistance versus backgate voltage for 60 μm wide sample and 4 - 15 μm long at 40mK.** (A) Sketch of two-terminal scheme. 1 nA was sourced (red contact) and drained to ground (blue contact). Downstream chiral edge states illustrated by solid arrows and upstream edge channels illustrated by dashed arrows. (B) 4 μm , (C) 5 μm , (D) 7 μm , (E) 10 μm , (F) 15 μm . (G) mean resistance of $\nu = 2/3$ unpolarized state (blue circles) and polarized state (orange circles, error bars are smaller than the circle size for some points), dashed black line represents the quantized value $(2/3 e^2/h)^{-1}$ and the blue dashed line is an exponential fit $R(x) = (R(0) - R(\infty)) e^{-x/l_0} + R(\infty)$, where $R(0) = 20 \pm 13 \text{ k}\Omega$, $R(\infty) = 38.2 \pm 0.3 \text{ k}\Omega$ and $l_0 = 2.1 \pm 0.8 \mu\text{m}$

3. Corbino geometry measurement

To probe directly the conductance of the bulk we designed a sample having a Corbino geometry as shown in Fig. S2A, the outer r_{out} and inner r_{in} radius are respectively 14 and 6 microns. Voltage (20 μV) is sourced in the inner contact and current is measured at the outer contact. The two terminal conductivity $\sigma = 1/2\pi \times \log(r_{out}/r_{in}) \times (I/V)$ is plotted in Fig. S2B. We can clearly see that both polarized and unpolarized $\nu = 2/3$ states are in a non-dissipative state.

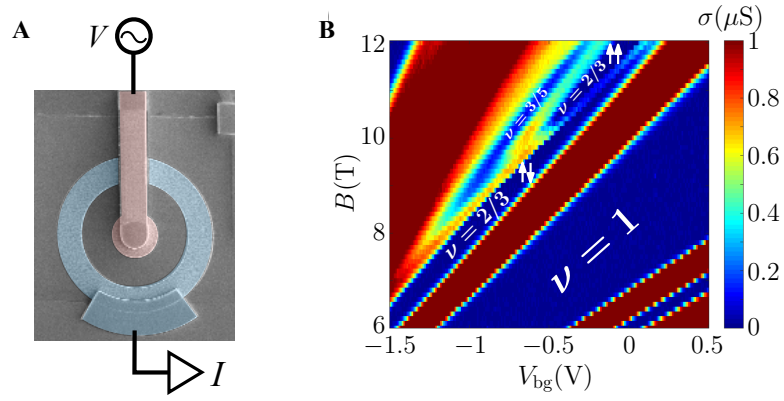


Figure 2: **Corbino geometry sample.** (A) Fake color SEM image of the corbino sample together with the measurement scheme, the blue colored ring shape ohmic contact has an inner radius of $14 \mu\text{m}$ and is connected to cold ground. The red colored part include a disc shape ohmic contact with radius of $6 \mu\text{m}$ and is connect to an air bridge. (B) Magnetoconductance measurement versus the backgate voltage. It is clear that both $\nu = 2/3$ polarized and unpolarized are in a non dissipative state showing that the bulk is incompressible in both cases.

4. Landauer-Buttiker formalism

Considering the system presented in Fig. S3A and Fig. S3B, one can calculate the upstream and downstream conductance using Landauer-Buttiker formalism [1, 2]:

$$\begin{pmatrix} V_1 \\ V_2 \\ V_3 \end{pmatrix} = [R] \begin{pmatrix} I_1 \\ I_2 \\ I_3 \end{pmatrix} = \begin{pmatrix} R_{11} & R_{12} & R_{13} \\ R_{21} & R_{22} & R_{23} \\ R_{31} & R_{32} & R_{33} \end{pmatrix} \begin{pmatrix} I_1 \\ I_2 \\ I_3 \end{pmatrix}$$

where

$$[R] = \begin{pmatrix} G_{12} + G_{13} + G_{14} & -G_{12} & -G_{13} \\ -G_{21} & G_{21} + G_{23} + G_{24} & -G_{23} \\ -G_{31} & -G_{32} & G_{31} + G_{32} + G_{34} \end{pmatrix}^{-1}$$

Inversing the matrix and replacing $G_{41} = G_{12} = G_{23} = G_{34} \equiv G_d$, $G_{14} = G_{21} = G_{32} \equiv G_u$ and $G_{13} = G_{31} = G_{24} = 0$ one finds the downstream resistance, which is the voltage measured downstream divided by the current:

$$R_{12} = \frac{V_1}{I_2} \equiv R_d = \frac{G_d}{G_u^2 + G_d^2}$$

and the upstream resistance which is the voltage measured upstream divided by the current:

$$R_{21} = \frac{V_2}{I_1} \equiv R_u = \frac{G_u}{G_u^2 + G_d^2}$$

one can find the upstream and downstream conductances:

$$G_d = \frac{R_d}{R_d^2 + R_u^2}$$

$$G_u = \frac{R_u}{R_d^2 + R_u^2}$$

In Fig. S3C and D, we plotted R_u and R_d directly from the 3-terminal measurement schemes presented in Fig. S3A and B respectively. We found $R_u = 1.42 \text{ k}\Omega \pm 0.07 \text{ k}\Omega$ and $R_d = 37.6 \text{ k}\Omega \pm 0.1 \text{ k}\Omega$ where value and the errors are the mean and standard deviation of the 2/3 unpolarized region. Next, we plot the upstream and downstream conductances in Fig. S3E and F, where we get the a mean value for the conductances in the unpolarized region $G_u = 0.026 e^2/h \pm 0.001 e^2/h$ and $G_d = 0.687 e^2/h \pm 0.002 e^2/h$.

Since not all of the contacts have the same distance from one another and since we claim the conductance of the 2/3 unpolarized state depend on the distance, we also made another calculation. Taking into consideration different conductance between contacts 3 and 4 which has much larger distance $\sim 70\mu\text{m}$ where the edge modes are fully equilibrated. Solving similar equations as above, plugging the same values of R_u and R_d and taking the equilibrated quantized value for $G_{34} = 2/3 e^2/h$ we get the same values for G_u and G_d as the approximated ones up to our measurement error.

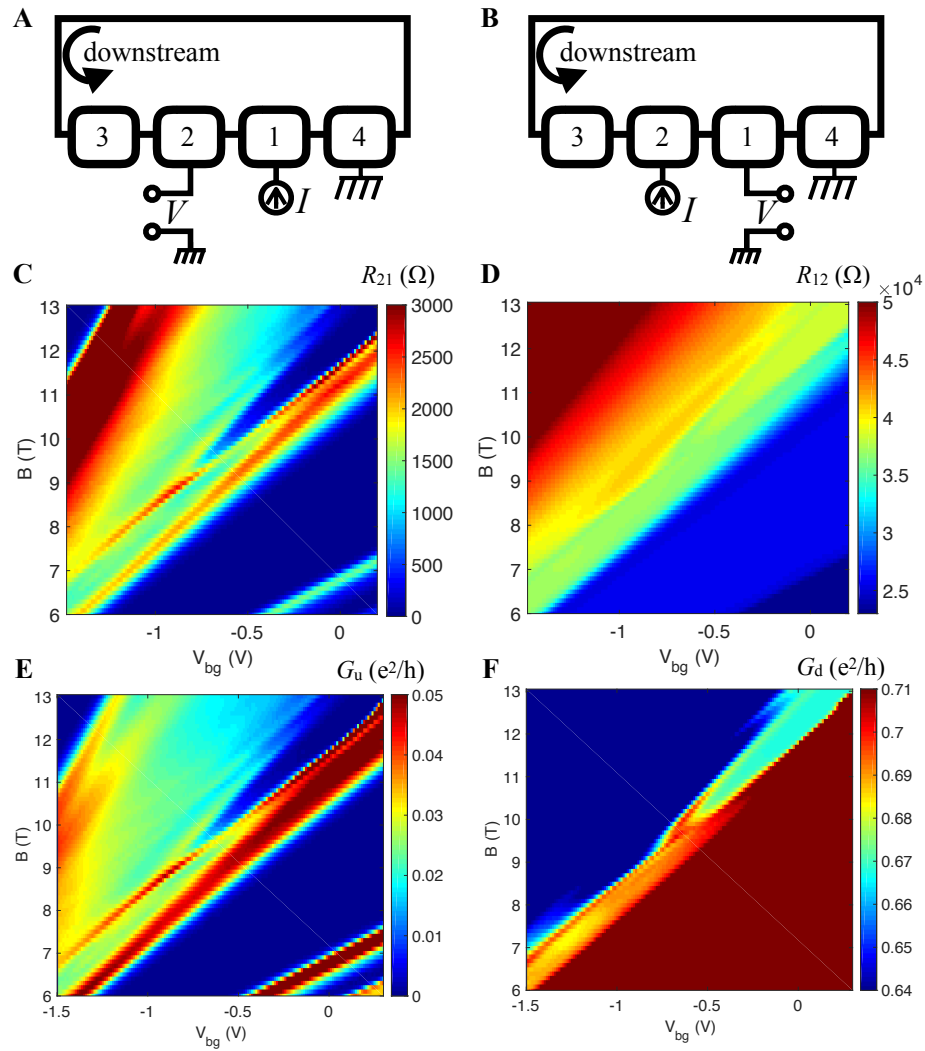


Figure 3: **Landauer-Buttiker analysis.** (A) 3-terminal upstream measurement scheme, 1 nA is sourced at contact 1 while voltage was measured at contact 2, upstream. Contact 4 was grounded and contact 3 was floating and wasn't in use. (B) 3-terminal downstream measurement scheme, 1 nA is sourced at contact 2 while voltage was measured at contact 1, downstream. Contact 4 was grounded and contact 3 was floating and wasn't in use. (C) upstream resistance measurement for the scheme presented in (A). (D) downstream resistance measurement for the scheme presented in (B). (E) upstream conductance calculated using L-B formalism $G_u = \frac{R_u}{R_d^2 + R_u^2}$. (F) downstream conductance calculated using L-B formalism

$$G_d = \frac{R_d}{R_d^2 + R_u^2}.$$

5. Current conservation

In the two QPCs configuration shown in Fig. S4C, we sourced 1 nA in contact S and measured current in all of the drains separately. In Fig. S4A, We plot the current measured in the downstream drains $D1 + D2$ as function of the two QPCs split gate voltages. In Fig. S4B, we plot the current measured in drain $D3$. We observe a reduction of the current in the downstream drains when upstream current is observed in $D3$. Overall yielding total current conservation in all drains $D1$, $D2$ and $D3$.

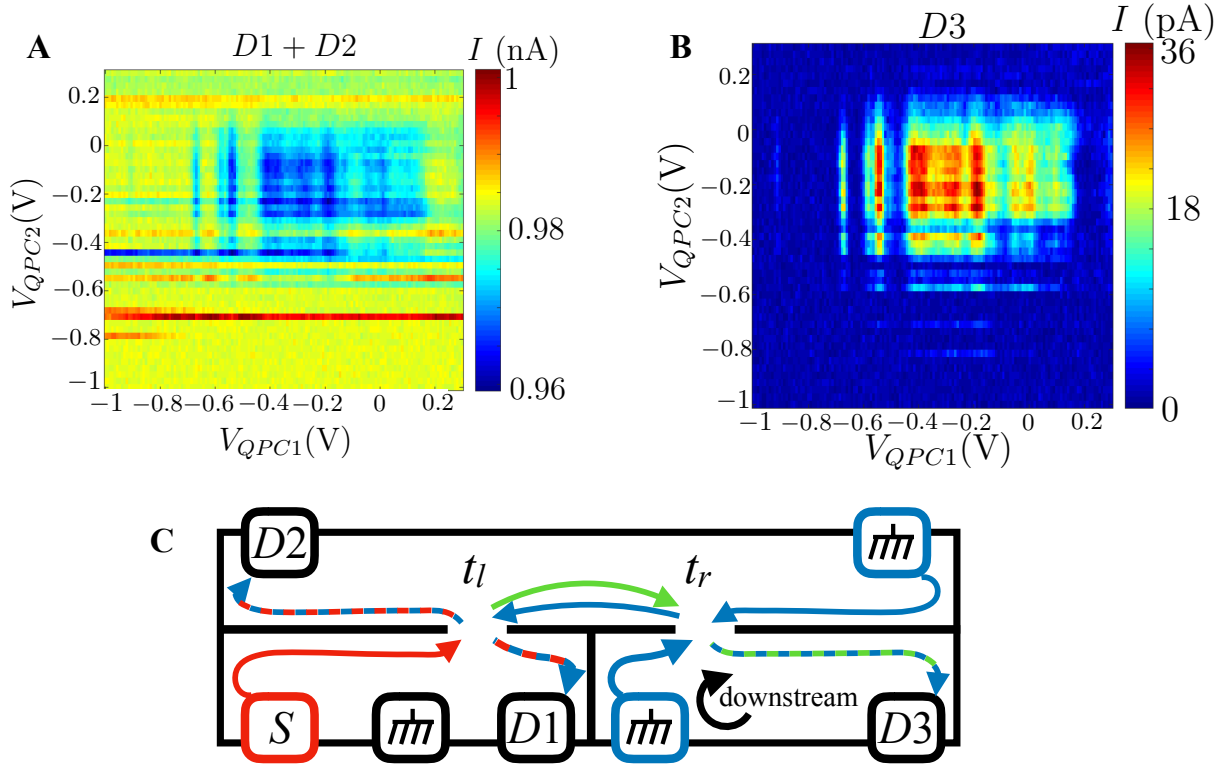


Figure 4: **Current conservation in two-point-contacts configuration.** (A) Sum of the current measured in $D1 + D2$ as function of the split gate voltages. (B) current measured in $D3$ as function of the split gate voltages. (C) Two successive quantum point contacts setup. Current is sourced in S (red), flowing downstream to the left QPC, there it is split to downstream (red/blue) and upstream (green) charge currents. The unequilibrated upstream current reaches the second QPC and turns back to downstream (green/blue) - measured in $D3$. Distance between the two QPC is 700nm and the distance between the QPC and the nearest ohmic contact is 30 μm (sketch not to scale).

6. Toy model for upstream current in two QPCs setup

This toy model predicts the amount of current flowing into $D3$ in the presence of upstream current. We modeled the two QPCs at half transmission by two metallic ohmic contact, which have equilibrium voltages V_l and V_r as shown in Fig. S5. Current I sourced in S (red) reaches the left contact (green). From the left contact we get one equilibrated downstream mode flowing long distance to $D1$ with conductance $2/3 e^2/h$, another equilibrated downstream mode flowing long distance to $D2$ with conductance $2/3 e^2/h$ and one unequilibrated upstream mode with conductance G_u flowing a short distance (700 nm) to the right contact. Current conservation on both contact yields:

$$\begin{aligned} I + V_r G_d &= V_l (2G_{2/3} + G_u) \\ V_l G_u &= V_r (G_d + G_{2/3}) \end{aligned}$$

where G_d and G_u are the unequilibrated downstream and upstream conductance and $G_{2/3} = 2/3 e^2/h$ is the equilibrated conductance. The current measured in $D3$ is $I_3 = V_r G_{2/3}$

$$I_3 = \frac{G_u I}{2G_{2/3} + 2G_d + G_u}$$

For example, for Macdonald's model [3] $G_d = e^2/h$, $G_u = 1/3e^2/h$ and $G_{2/3} = 2/3e^2/h$ we get $I_3/I \approx 0.09$, about three times higher value than what we measured. We didn't take into consideration any specific mechanism which convert dissipation at the QPC to upstream modes, furthermore, one can take into account different transmissions in the QPCs, where the model presented here takes only half transmission. The highest signal of upstream current we measured in correspondence with the highest dissipation occurring in a QPCs, where $t_l = t_r = 1/2$.

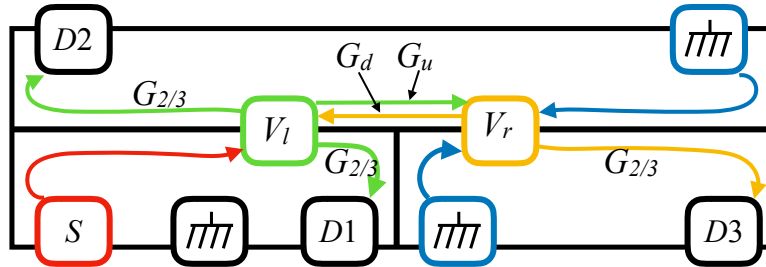


Figure 5: **Toy model sketch.** The two QPCs were replaced by ohmic contacts which acquire a voltage V_l and V_r . The short distance between the two ohmic contacts (700 nm) give rise to equilibrated edge modes propagating upstream and downstream flowing between the two. Other edge modes are in full equilibration due to long distance, above $30 \mu\text{m}$ (sketch not to scale).

-
- [1] M. Büttiker. Four-Terminal Phase-Coherent Conductance. *Physical Review Letters*, 57(14):1761–1764, oct 1986.
 [2] Supriyo Datta. *Electronic Transport in Mesoscopic Systems*, volume 3. 1995.
 [3] A. H. MacDonald. Edge states in the fractional-quantum-Hall-effect regime. *Physical Review Letters*, 64(2):220–223, jan 1990.